Investigation of the seismic fault that ruptured during the 7/9/99 Athens earthquake using space techniques

Ganas[1], A., Stavrakakis[1], G., Lagios[2], E., Papadopoulos[1], G., & Pavlides[3], S.

[1]Geodynamics Institute, National Observatory of Athens, PO Box 20048, 118 10 Athens, Greece. aganas@gein.noa.gr

[2]University of Athens, Geology Dept., 157 84 Panepistimiopolis, Athens, Greece.

[3]Aristotle University of Thessaloniki, Geology Dept., 54 006, Thessaloniki, Greece.

ABSTRACT

The 7/9/1999 Athens earthquake (5.9 Ms) caused only gravitational breaks and numerous tension cracks, rock falls and other shaking phenomena, without any surface ruptures. Despite the good agreement in the focal plane solutions (NP1: 110-130, 50-70° SW) ambiguities in epicentre position and depth rendered the location of the seismic fault as debatable. Here we employ digital image processing techniques using a combination of Differential Interferometry, Landsat TM satellite data, Digital Elevation Models (DEMs) and vector layers comprising our field observations to show that the NW-SE striking, SW-dipping Fili normal fault ruptured during this event.

INTRODUCTION

We used a combination of space techniques to determine the seismic structure that moved during the 7/9/1999 5.9 Ms earthquake (Pavlides *et al*., 1999; Papadopoulos *et al*., 2000; Figure 1): a) interpretation of Landsat TM images (Figure 2), b) processed digital topography (Figure 3) and c) SAR interferometry (Figure 4). The interpretation of the infrared bands of the Landsat data was directed towards understanding the spatial properties of landforms including: the patterns of undisturbed alluvial fans and transverse bedrock ridges, the sinuosity of linear features and the configuration of relief in the southern Parnitha mountain area. In general, linear mountain fronts and parallel drainage in the footwall of normal faults testify for recent activity (Ganas *et al*., 1998; Goldsworthy and Jackson, 2000). In the broader area to the NW of Athens (southern Parnitha Mountain area), the Landsat data allow the identification of two southwest-dipping normal fault segments, namely Thriassion and Fili. There is no other active structure to the north of those fault segments except for the E-W striking faults on the northern flanks of Parnitha. These observations are reproduced after examining shaded relief images. The ruptured segment is highlighted by the overlay of the aftershock sequence recorded by the local seismological network of the National Observatory of Athens as a vector layer (with x-y accuracy of ± 1000 m) on top the 20-m shaded relief imagery illuminated from the SE (Figure 3a) because we find that the majority of the population is plotted on the hangingwall of the Fili fault. In addition, by plotting the localities where effects of the earthquake were mapped (gravitational breaks, damages, rock falls) as point vectors (with x-y accuracy of ± 100 m), it is observed that almost all of them are aligned parallel to the strike of the Fili fault. Finally, interferometric processing of radar imagery was used to map the extent of the deformation field following the earthquake. Some details of the image processing are reported below.

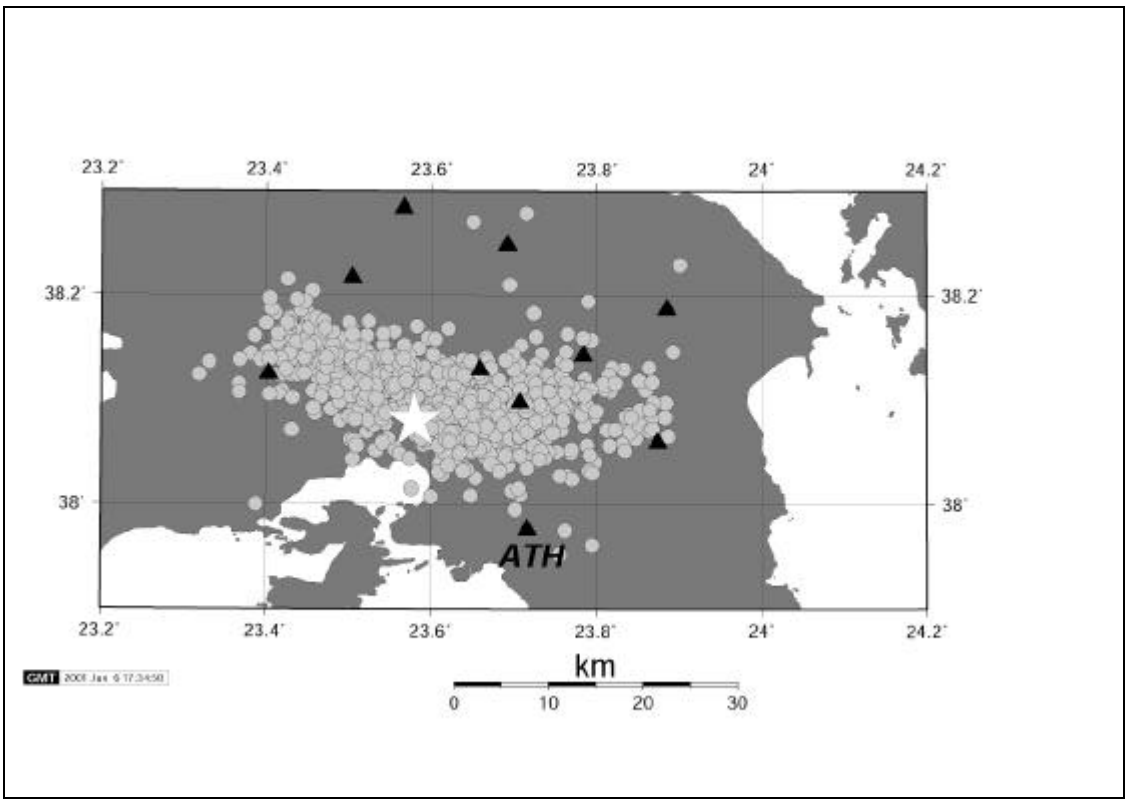

Figure 1. Map showing the epicentre distribution of the aftershock sequence of the Athens earthquake (7/9/99, 5.9 Ms). Bright star denotes the epicentre of the mainshock. Black triangles are the positions of the local, analogue seismological network operated by the National Observatory of Athens during September-November 1999.

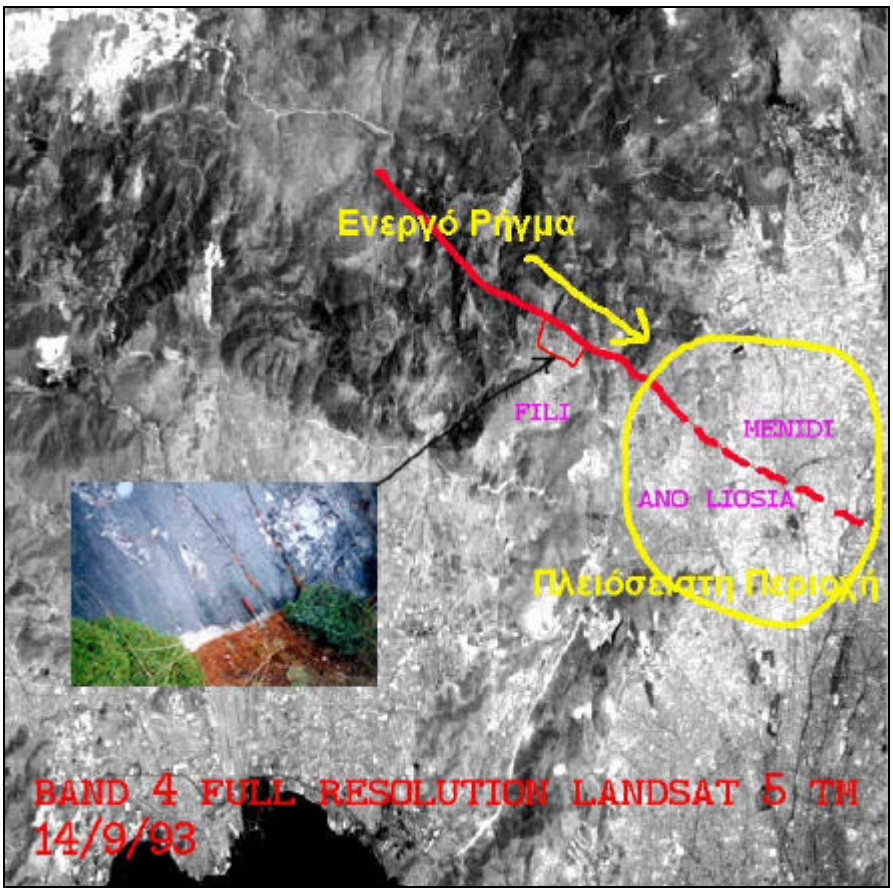

Figure 2. Landsat 5 satellite Image of the Athens earthquake area. The data are system-corrected (level 5) and band 4 (near infrared) is displayed. The red line indicates the location of the Fili normal fault. Inset field photograph shows a polished surface along the Fili Fault. Yellow ellipse shows extent of meisoseismal area. Yellow arrow shows directivity of rupture.

IMAGE PROCESSING

A standard method to visualize a seismogenic fault is to apply digital processing techniques to obtain either nadir or oblique, panoramic views of the greater area it deforms (Figures 2, 3). The views help to

1. Map the extent of the structure and measure its length. This is helpful to estimate various seismic parameters, such rupture length and associated maximum magnitude etc
2. Estimate cumulative offset along strike by identifying displaced ridges. The ridges may be also identified on a topographic map of the imaged area or on a Digital Elevation Model (DEM). This technique is used to estimate horizontal strain within a 10% margin and amount of extension by assuming a fixed angle of slip (usually 50-60 degrees).
3. To identify footwall (hangingwall) cross faults and
4. To study the long-term evolution of landforms in the meisoseismal area of the earthquake. This can be done by calculating geomorphic ratios, such as sinuosity indices, valley widths to valley lengths ratios etc.

The views provided by shaded relief images choosing various illumination conditions (Figure 3a; also Ganas *et al*., 2001a) depend on the DEM resolution and on the tectonic setting. The long-term evolution of normal-faulted terrains is assumed to result from accumulated co-seismic motions (uplift-subsidence) and erosion due to climatic variations (Armijo *et al*., 1986; Anders and Schlische, 1994). The shaded relief image of Figure 3a simulates a low sun angle (zenith=75°), southeastern viewing direction (140° clockwise of N) of the western Attica region in Greece. This image stems from a DEM of cartographic origin (HAGS, 1992) and can be used as a raster background to overlay vector files like the shallow aftershock sequence of the 7/9/1999 Ms 5.9 earthquake. A southeastern illumination accentuates topography better because in central Greece the predominant extension direction is north south (Clarke *et al*., 1998). The same image can also host damage information after the collection of field observations and other macroseismic data (Ganas *et al*., 2001b). Two normal faults can be identified (Thriassion and Fili) and the overlay of the aftershock sequence shows that Fili fits the pattern better.

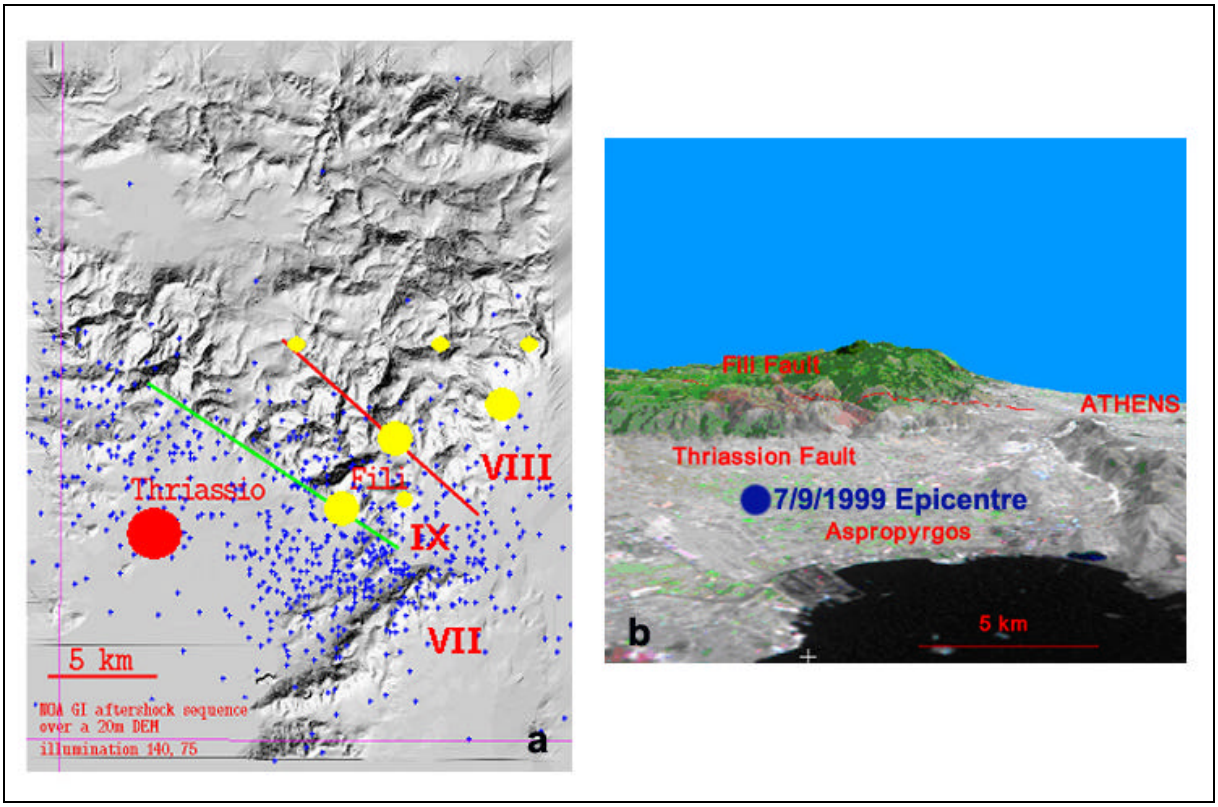

Figure 3a) Shaded relief image of a Digital Elevation model of the meisoseismal area simulating orientation of topography with respect to an illumination source (SE-140; zenith angle of 75 degrees). Green line is the Thriassion normal fault; red line is the Fili normal fault. Blue crosses are aftershock epicentres; red circle is the relocated NOAGI epicentre of the main shock of Sept. 7, 1999. Map shows also the distribution of rock falls (yellow circles). Roman capital letters indicate the earthquake intensity. **3b)** Perspective view (towards northeast at 35° above the horizon) of western Attica, Greece. The image was constructed using computer vision techniques, TM imagery (741 RGB) and a 20-m DEM. Red line is the trace of the Fili normal fault that moved during the 7/9/1999 earthquake. Vertical exaggeration x 3.

Secondly, oblique views were constructed to visualize the pattern of regional structures (Figure 3b) in the vicinity of the epicentre. Here a technique called ”draping” is applied, where a satellite image of comparable pixel size to a pre-existing DEM is overlain. The resulting file has been

rotated to a variety of viewing directions to make better observations of the fault pattern. An exaggeration of the topography is necessary to distinguish fault segmentation associated with slip deficits and low relief. In the case of Figure 3b fault segment boundaries may be identified on both ends of the Thriassion normal fault segment, and on the eastern end of the Fili normal fault segment in Attica, Greece. A vector layer, the trace of the Fili fault (red line), is also superimposed to show the exact location of the seismogenic structure. To accurately register DEMs and Landsat satellite data we used suitable grid spacing of the order of 10-to-20-m by on-screen digitising of elevation contours of the 1:50,000 map sheets (contour interval 20 m). However, the degree of co-registration needs to be better than one pixel of the satellite image.

SAR INTERFEROMETRY

The Interferometry technique (InSAR) has been applied to study the earthquake behaviour of active faults in various parts of the world including Greece (Massonnet *et al.*, 1993; Meyer *et al.*, 1996; Wright *et al.*, 1999, Kontoes *et al.*, 2000, Briole *et al*., 2000; see Figure 3). This mapping capability is possible on regional and even global scales using specialized, radar processing software. DEMs may be also created with height accuracies on the order of 5-20 metres. Detailed analysis of the phase part of the signal along the line of sight (slant range) can determine the surface displacement that has occurred between successive orbits of the satellite, even when the orbits are years apart. However, the technique works much better in flat and dry areas because of constraints in the imaging geometry (the ERS satellite has a high incidence angle, 23°) and the climatic influence on phase coherence since wet climatic conditions cause quick, temporal decorrelation of the phase returns. Coherence in the study area is maintained better on the flat areas of Thriassion and Athens basins than on the Parnitha Mountain.

In this study we used the ATLANTIS software for Windows NT (version 1.2.1) where we applied the 2-pass method (Figure 4) involving a) resampling of the external DEM to the master SAR image (ERS-2 orbit 23136 – 23 September 1999), b) distortion of the re-sampled DEM creating foreshortening and layover distortions c) fine, interactive co-registration of the DEM to the master SAR image using more than 20 tie points with residuals less than a pixel d) calculation and subtraction of the topographic phase from the interferogram. The phase unwrapping is done by the use of the iterative disk-masking algorithm (copyright of ATLANTIS) with controlled error propagation and error correction. The algorithm uses multiple tiling and seeding techniques. The best pair has an altitude of ambiguity of 67 m and a time difference of 68 days. The external DEM is the same used in Figure 3 with a grid size of 20 metres and vertical accuracy of 5 metres. Neither remaining topographic phase nor atmospheric effects were detected on the interferogram. Two phase cycles (fringes) can be seen from the coastline to the centre of the image with the following colour succession: red-blue-green-red. This succession shows a negative phase cycle (subsidence). Also, the pattern of extracted fringes shows an N110-N120 axis of the deformation ellipse, parallel to the Fili neotectonic fault in agreement with geological and seismological data (Pavlides *et al*., 1999, Papadopoulos *et al*., 2000). The calculated height-change map (the vertical component of the line-of-sight vector) shows that the area of subsidence ranges between 2-7 cm with the maximum observed in the greater area of the ancient Fili Fort. Subsidence of 2-4 cm also occurred in the Ano Liossia Area of the Athens basin where extensive damages and loss of life occurred. An area of uplift at the bottom centre (near the coastline) is so marginal (3-8 mm) that lies within the limits of error. We note that these results differ by those of Kontoes *et al*., (2000) in that the ellipticity of our fringes is greater. This may imply a steeper geometry of the seismic source so that the intersection of the fault plane with the free surface correlates better with the mapped Fili fault of Pavlides *et al*., (1999). However, no GPS data exist to measure the co-seismic deformation of the Athens earthquake so this point (kinematics) needs further investigation.

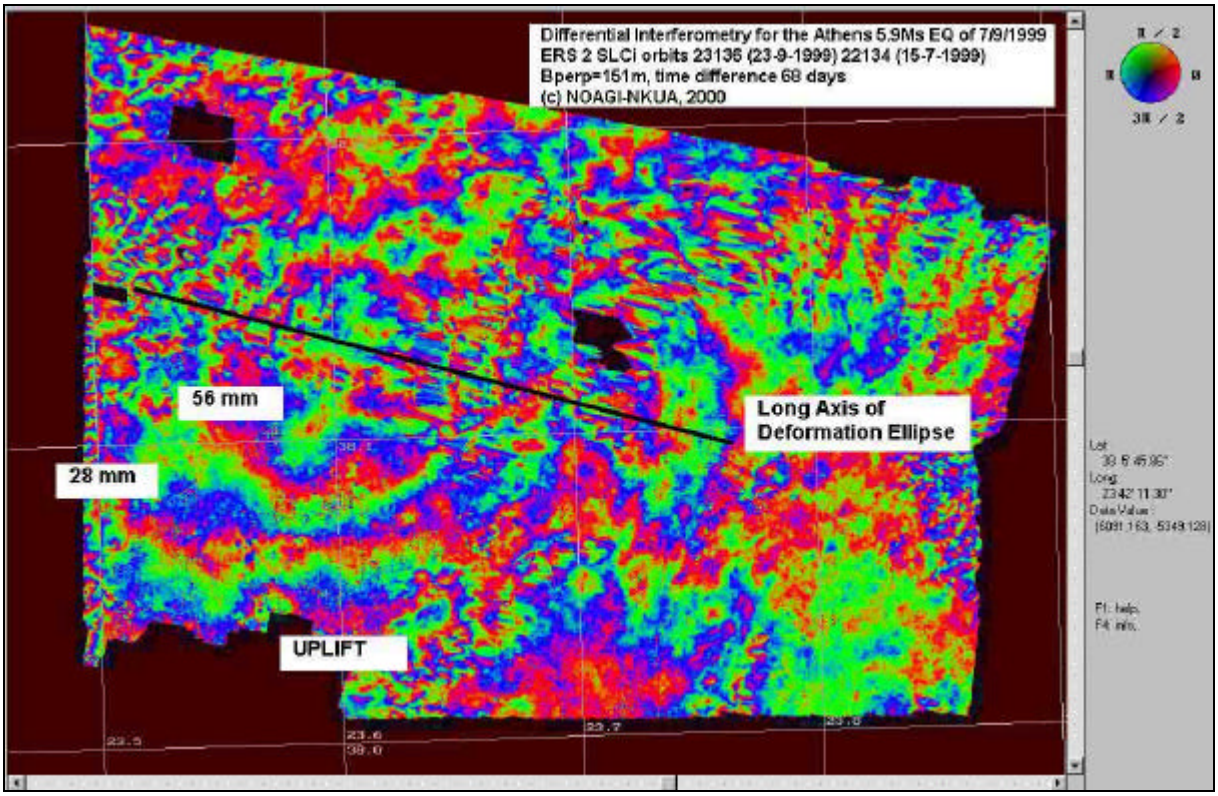

Figure 4. Image showing the interferogram of the Athens earthquake from the phase difference (in slant range) of two ERS 2 satellite images. Time difference is 68 days and the perpendicular baseline between the two orbits is 151 metres. An external digital elevation model with 20-m resolution was used to subtract pre-existing topography. Two elliptical fringes can be distinguished; the internal one labeled 56 mm, while the external 28 mm. Figures are amounts of subsidence. Black patches are areas of low coherence.

DISCUSSION-CONCLUSIONS

Remote sensing can provide conclusive evidence towards identifying the surface expression of seismogenic structures during events in the range 5.5 to 6 Ms. Because of the limited appearance or even non-existence of primary effects of the earthquake (e.g., surface ruptures) during many of the above events, DEM resolution and sun angle are the dominant factors that influence mapping quality. Two-pass differential interferometry can provide 1:50000 scale maps of the full, coseismic deformation field for events exceeding 5.8 Ms.

In this study, the identification of two southwest-dipping normal fault segments, Thriassion and Fili, was confirmed using 3D visualization techniques on satellite imagery and DEMs. No other active structure was detected towards the north. The ruptured segment is indicated by the overlay of the NOA aftershock sequence as a vector layer on top of monochromatic TM imagery and the shaded relief imagery. Almost all aftershocks are plotted on the hangingwall of the Fili fault. In addition, by plotting the localities where effects of the earthquake were mapped (gravitational breaks, damages, rock falls), it is observed that almost all of them are aligned parallel to the strike of the Fili fault. This fault also fits better the deformation pattern mapped by differential interferometry.

Acknowledgements

We thank Geoff Wadge, Gerald Roberts, Kevin White, Martha Stefouli, Isaak Parcharidis, Tim Wright, Haris Kontoes, Alexis Rigo, Pepi Vasilopoulou, Vassilis Sakkas, Vassilis Karastathis and the ATLANTIS support team for discussions and comments. IIS SA provided TM images and the EASI PACE software for the production of Figures 2 and 3. This work was partially funded by the GEOWARN project (IST 1999-12310).

REFERENCES

Anders, M. H., and Schlische, R. W., 1994. Overlapping faults, intrabasin highs, and the growth of normal faults. *Journal of Geology*, **102**, 165-180.

Armijo, R., Tapponier, P., Mercier, J. L., and Tong-Lin, H., 1986. Late Cenozoic right-lateral strike-slip faulting in southern Tibet: Field observations and tectonic implications. *Journal of Geophysical Research*, **91**(B14), 13803-13872.

Briole, P., Rigo, A., Lyon-Caen, H., Ruegg, J. C., Papazissi, K., Mitsakaki, C., Balodimou, A., Veis, G., Hatzfeld, D., and Deschamps, A., 2000. Active deformation of the Corinth Rift, Greece: results from repeated Global Positioning System surveys between 1990 and 1995. *Journal of Geophysical Research*, **105** (B11), 25605-25625.

Clarke, P. J., Davies, R. R., England, P. C., Parsons, B., Billiris, H., Paradissis, D., Veis, G., Cross, P. A., Denys, P. H., Ashkenazi, V., Bingley, R., Kahle, H. G., Muller, M. V., and Briole, P., 1998. Crustal strain in central Greece from repeated GPS measurements in the interval 1989-1997. *Geophysical Journal International*, **135**, 195-214.

Ganas, A., Lagios, E., and Stavrakakis, G., 2001a. Computer techniques for imaging earthquake deformation using satellite data and digital elevation models. Proceedings of 9th Congress of the Geological Society of Greece.

Ganas, A., Papadopoulos, G., and Pavlides, S. B., 2001b. The 7th September 1999 Athens 5.9 Ms earthquake: remote sensing and digital elevation model inputs towards identifying the seismic fault. *International Journal of Remote Sensing*, **22** (1), 191-196.

Ganas, A., Roberts, G. P., and Memou, Tz. 1998. Segment boundaries, the 1894 ruptures and strain patterns along the Atalanti Fault, Central Greece. *Journal of Geodynamics*, **26**(2-4), 461 - 486.

Goldsworthy, M., and Jackson, J., 2000. Active normal fault evolution in Greece revealed by geomorphology and drainage patterns. *Journal of the Geological Society*, **157**, pp. 967-981.

Hellenic Army Geographical Service, 1992. Map Sheet "Elefsis".

Kontoes, C., Elias, P., Sykioti, O., Briole, P., and Remy, D., 2000. Displacement field and fault model for the September 7, 1999 Athens earthquake inferred from ERS2 satellite radar interferometry. Geophysical Research Letters, **27**, 24, p. 3989.

Massonnet, D., Rossi, M., Carmona, C., Adragna, F., Peltzer, G., Feigl, K., and Rabaute, T., 1993. The displacement field of the Landers earthquake mapped by radar interferometry. **Nature**, **364**, 138-142.

Meyer, B., Armijo, R., Massonnet, D., de Chabalier, J. B., Delacourt, C., Ruegg, J. C., Achache, J., Briole, P., and Papanastasiou, D., 1996. The 1995 Grevena (northern Greece) earthquake: fault model constrained with tectonic observations and SAR interferometry. *Geophysical Research Letters*, **23**, 2677-2680.

Papadopoulos, G. A., Drakatos, G., Papanastassiou, D., Kalogeras, I., Stavrakakis, g., 2000, Preliminary results about the catastrophic earthquake of 7 September 1999 in Athens, Greece. *Seismological Research Letters,* **71**, 318-329.

Pavlides, S., Papadopoulos, G. A., and Ganas, A., 1999. The 7th September 1999 unexpected earthquake of Athens: Preliminary results on the seismotectonic environment, 1st Conf. Advances in Natural Hazards Mitigation: Experiences from Europe and Japan, Programme-Abstracts-Reports, Athens, 3-4 November 1999, 80-85.

Wright, T. J., Parsons, B. E., Jackson J. A., Haynes, M., Fielding, E. J., England, P. C., and Clarke, P. J., 1999. Source parameters of the 1 October 1995 Dinar (Turkey) earthquake from SAR Interferometry and seismic bodywave modeling. *Earth and Planetary Science Letters,* **172**(1-2), 23-37